JACS
JOURNAL OF THE AMERICAN CHEMICAL SOCIETY
pubs.acs.org/JACS
Article

Probing Spatial Energy Flow in Plasmonic Catalysts from Charge Excitation to Heating: Nonhomogeneous Energy Distribution as a Fundamental Feature of Plasmonic Chemistry

Rachel C. Elias, Bill Yan, and Suljo Linic*

Cite This: J. Am. Chem. Soc. 2024, 146, 29656−29663
Read Online

ABSTRACT: Plasmonic catalysts use light to drive chemical reactions. One critical question is how light energy moves at nanoscales in these complex systems, leading to chemical transformations. In this contribution, we map out this energy flow by developing approaches to measure spatial temperature distributions in heterogeneous plasmonic catalysts, consisting of three-dimensional networks of plasmonic nanoparticles anchored on an oxide support. We survey the local temperatures of molecules adsorbed on catalytically active plasmonic nanoparticles, the nanoparticles themselves, and the catalyst support, under steady-state continuous-wave illumination. We reveal the existence of large temperature gradients, in which the local temperatures of the molecules, nanoparticles, and the surrounding environment can vary greatly. We show that these temperature gradients are a natural consequence of plasmon relaxation, involving the interconversion between electromagnetic light energy, electronic excitations, and heating of various entities as these electronic excitations relax. The presence of these gradients is a fundamental and unique feature of gas-phase plasmonic catalysis.

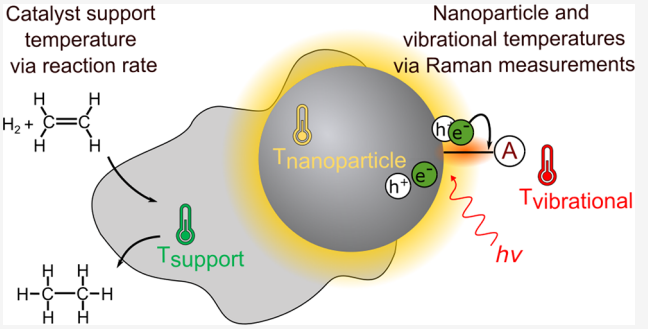

INTRODUCTION

Plasmonic catalysis leverages the localized surface plasmon resonance (LSPR) of metal nanoparticles (e.g., Ag, Au, and Cu) to drive chemical reactions under UV−vis light illumination.[1−5] Although there have been numerous advances in the design and applications of plasmonic catalysts, the mechanism by which energy is exchanged between a plasmonic nanoparticle and the rest of the system, including an attached reacting adsorbate or optically and chemically inert support material in functioning systems, is still under debate.[6−10] Based on extensive experimental and computational studies, it is clear that plasmons relax via an excitation of energetic electron−hole (e/h) pairs of LSPR energy.[11−15] The rates of these plasmon relaxation processes at specific atomistic locations are governed by the local dielectric function and the intensity of the local, plasmon-induced electric fields.[1,16−19] In simple terms, the local regions of a plasmonic catalytic system with a high imaginary part of the dielectric function will yield higher rates of e/h pair formation, subject that there are local fields that can drive the plasmonic energy to these locations.

In plasmonic catalysis, these excitations of energetic e/h pairs induce chemical transformations. For example, in gas phase plasmonic reactions, the relaxation ("cooling") of energetic e/h pairs through their interactions with vibrational modes of the system can result in heating of the catalyst or a selective vibrational heating of reactants which can result in chemical transformations.[1,8,16,20−22] An argument that is often made in the literature, that there are two mutually exclusive mechanisms for driving gas-phase plasmonic chemical reactions (the heating and charge excitation mechanisms), is imprecise since the formation of energetic e/h pairs (charge excitation) is *the only* initial driver for a reaction.[20] A more credible question is whether the above-discussed nonhomogeneous rates of e/h formation can result in nanoscopic temperature gradients, where the adsorbate (reactant) may not be in thermal equilibrium with the catalyst but instead is at a higher temperature (Figure 1). For example, if electronic excitations and their "cooling" through coupling to the phonon modes take place exclusively within plasmonic nanoparticles, then these nanoparticles essentially act as local nano heaters. In this scenario, adsorbates (reactants) on the nanoparticles can gain energy and chemically react only via a thermal equilibration with the nanoparticles. Under these conditions, the nanoparticles and reactants would be at the same steady state temperature, as illustrated in the top portion of Figure 1.

Received: July 30, 2024
Revised: October 6, 2024
Accepted: October 8, 2024
Published: October 16, 2024

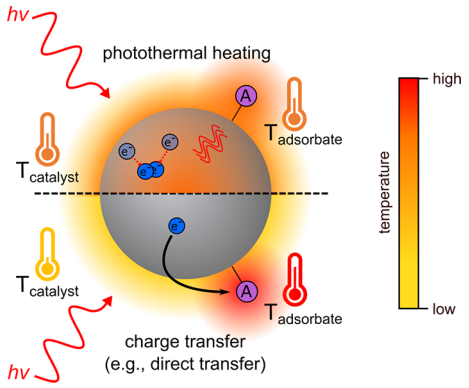

Figure 1. Illustration of two energy transfer pathways for photomediated chemistry on a plasmonic metal nanoparticle catalyst. In the photothermal heating pathway (top half), the initial generation and relaxation of charge carriers in the nanoparticle are required to subsequently heat the nanoparticle and surrounding environment (catalyst support, adsorbates, etc.) and induce reactions. By comparison, the charge excitation mechanism (bottom half) assumes excited charge carriers directly interacts with the adsorbate, heating the reactant molecule and leading to chemical reactions. The local temperature distribution can be unique for the different scenarios.

Alternatively, a related question is whether it is possible to have situations where molecules anchored on plasmonic nanoparticles (i.e., the reactants) can be at elevated temperatures compared to the nanoparticles and the rest of the system, as shown in the bottom portion of Figure 1. This would be the case if there are electronic excitation processes localized on adsorbates, i.e., if the nanoparticle acts as an antenna, confining the electromagnetic energy to its surface. In this scenario, chemical reactions can be facilitated by this localized heating of adsorbates, as opposed to the equilibrium heating of the entire system. The existence of these temperature gradients would make plasmonic catalytic systems unique relative to classical catalytic systems, where the temperature differences between adsorbate, catalyst, and support are negligible due to bulk heating by convection and conduction.

To answer these questions, the local temperatures of various entities in a functioning plasmonic catalyst system under steady state conditions need to be characterized. In this contribution, we develop and implement approaches to characterize the temperature of these components. We illustrate the approach in the case study of a ∼ 6 wt % Ag/α-Al_2O_3 plasmonic catalyst, consisting of ∼60 nm diameter Ag nanoparticles dispersed across the α-Al_2O_3 oxide support, in a reactive flow system. We specifically focus on an oxide-supported heterogeneous catalytic system, since these remain the industry standard for gas-phase catalytic applications. We measure the local temperature of the following components:

1. **$T_{support}$: The temperature of the catalyst support sites** (in this case, α-Al_2O_3) was assessed by measuring the rate of a thermal chemical reaction that can take place only on the oxide support material and not on the plasmonic Ag nanoparticles. The reaction rate is connected to the temperature through a well-established Arrhenius rate/temperature dependence. Specifically, we studied the rate of C_2H_4 hydrogenation.[23] The C_2H_4 hydrogenation takes place only on the α-Al_2O_3 support and not on Ag, making it uniquely suited to quantify the local temperature of the α-Al_2O_3 sites with and without light illumination.
2. **$T_{nanoparticle}$: The local temperature of the Ag nanoparticles** under relevant conditions was measured using Raman anti-Stokes nanothermometry.[21,24−26]
3. **$T_{vibrational}$: The vibrational temperature of an adsorbate on the nanoparticle surface** was measured by using the ratio of anti-Stokes and Stokes Raman excitations of a probe molecule, rhodamine 6G (Rh6G), absorbed on the Ag nanoparticles. This ratio was compared to the thermal Boltzmann distribution-predicted value.[21,27−29] Using this approach, we characterized the temperature of adsorbed Rh6G under visible light illumination.

Our data and analysis show that local electronic excitations, induced by the relaxation of LSPR, can lead to substantial nanoscopic temperature gradients in reactive plasmonic catalytic systems, where the local temperatures of the attached molecule, nanoparticles, and surrounding environment can vary significantly even under steady state continuous wave illumination. These variations suggest that localized effects play a significant and unique role in plasmonic catalysis.

EXPERIMENTAL SECTION

Ag nanoparticles (prepared via a colloidal method, producing particles of roughly ∼60 nm diameter) and the 6 wt % Ag/α-Al_2O_3 catalyst were prepared following a procedure reported previously.[7,30,31] Details of the synthesis and characterization of the catalyst are provided in the Supporting Information. We note that this catalyst exhibits low to moderate nanoparticle clustering, as quantified and described in our earlier work.[7] All catalysts were calcined in air at 250 °C for 3 h to remove the polymeric stabilizer, and subsequently reduced under 20% H_2 at the same temperature for an additional 3 h. We utilized an annular quartz tube photoreactor previously designed in our lab to conduct the C_2H_4 hydrogenation reaction studies. More details of the reactor are provided in our previous publication and the Supporting Information.[7] The reactant stream for C_2H_4 hydrogenation experiments consisted of 10% C_2H_4 and 75% H_2 in balance N_2 and was introduced to the reactor for 10 h (overnight) prior to collecting data.

For all Raman experiments, which were used to measure the nanoparticle and molecular temperatures, we utilized the 6 wt % Ag/α-Al_2O_3 catalyst with and without the presence of adsorbate molecules. We employed the Rh6G adsorbate molecule since it displays a characteristic absorbance peak at 532 nm (Figure S6A), which overlaps with the Ag plasmon. To functionalize the Ag nanoparticle surface with Rh6G, we incubated a solution of the nanoparticles with 40 μM Rh6G overnight prior to preparing supporting the particles on α-Al_2O_3. Upon modifying the nanoparticle catalyst with Rh6G, the diffuse reflectance spectrum of the catalyst under N_2 confirmed a strong optical extinction peak near 532 nm, corresponding to Rh6G (Figure S6B). All Raman studies were performed in a Harrick high temperature reaction chamber.[8,21]

RESULTS AND DISCUSSION

Reaction Rate as a Tool to Characterize Catalyst Support Temperature ($T_{support}$). We begin with the analysis of the temperature of the α-Al_2O_3 support ($T_{support}$). We used the measured rate of C_2H_4 hydrogenation as a tool to probe the α-Al_2O_3 temperature on the 6 wt % Ag/α-Al_2O_3 catalyst. C_2H_4 hydrogenation was chosen as the probe reaction since it is thermally catalyzed by the α-Al_2O_3 support, whereas Ag surfaces do not catalyze the reaction under these conditions.[23,32] Therefore, the measured change in the reaction rate can be correlated to the temperature of the α-Al_2O_3 sites using the Arrhenius rate/temperature dependence. To confirm that the α-Al_2O_3 sites were the only active sites for the

https://doi.org/10.1021/jacs.4c10395
J. Am. Chem. Soc. 2024, 146, 29656−29663

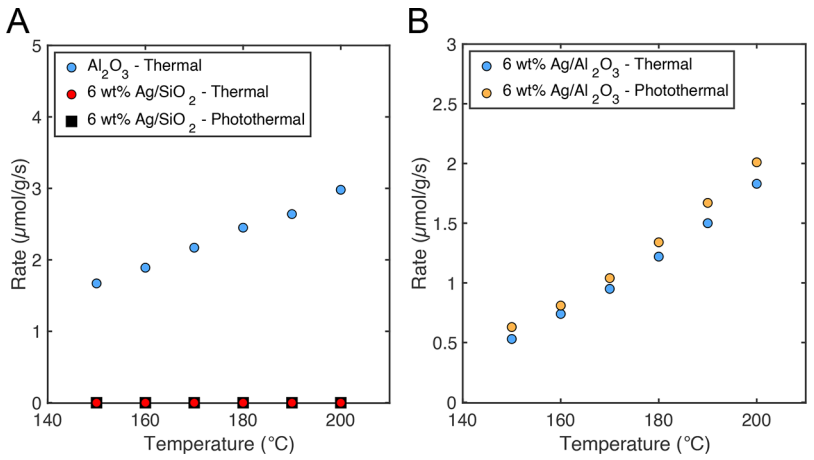

Figure 2. Thermal and photothermal reaction rates for α-Al_2O_3-driven C_2H_4 hydrogenation. (A) Measured reaction rates on bare α-Al_2O_3, which facilitates the reaction, and 6 wt % Ag/SiO_2, which exhibits no conversion under thermal and photothermal conditions. (B) Measured reaction rates on 6 wt % Ag/α-Al_2O_3 show low enhancement between thermal and photothermal conditions. All rates are plotted per gram of α-Al_2O_3. Photothermal data were collected under a light intensity of 400 mW/cm^2.

reaction, we first measured the rates of the reaction on the bare α-Al_2O_3 support (no Ag) in an annular photoreactor described previously and further in the Supporting Information.[7,33] The data in Figure 2A show the reaction rates on the bare α-Al_2O_3 support, confirming that the material is active for the hydrogenation reaction. To independently confirm that the Ag nanoparticles are not active for the hydrogenation reaction, we also measured the hydrogenation rates for a 6 wt % Ag/SiO_2 catalyst (where the Ag nanoparticles were supported on SiO_2 instead of α-Al_2O_3) prepared in an otherwise identical manner to the Ag/α-Al_2O_3 catalyst. The data in Figure 2A, in red, confirm that over the Ag/SiO_2 catalyst there was no conversion of the reactants and that the Ag nanoparticles do not facilitate the reaction.

We next compared reaction rates under thermal (dark) and photothermal (illuminated) conditions on 6 wt % Ag/α-Al_2O_3 to characterize the potential temperature increase under illumination for the α-Al_2O_3 support sites ($T_{support}$). We used a broadband light intensity of 400 mW/cm^2 and the reactant composition specified in the Methods section. The data in Figure 2B show that the plasmonic rate enhancement (i.e., the increase in rate between thermal and photothermal conditions at the same external thermal input) for the 6 wt % Ag/α-Al_2O_3-catalyzed C_2H_4 hydrogenation is very low. In other words, the photothermal rates on 6 wt % Ag/α-Al_2O_3 are only marginally higher than the thermal rates on the same catalyst. This essentially means that for this Ag loading, there is no significant heating of the α-Al_2O_3 support by the Ag nanoparticles. We note that in general, in plasmonic catalysis with Ag where the reaction is driven by the illuminated Ag nanoparticles, the light-induced rate enhancements for similar light intensities and catalysts are multifold.[1,7,31] The low C_2H_4 hydrogenation rate enhancement under light suggests that the support sites for this 6 wt % Ag/α-Al_2O_3 catalyst undergo very little heating under illumination (we estimate no more than 10 degrees). In line with this, we also observed no statistically significant changes in the activation barrier for the reaction between thermal (41 ± 3 kJ/mol) and photothermal (39 ± 1 kJ/mol) conditions.

We note that the hydrogenation reaction-measured extent of heating of the α-Al_2O_3 support sites on the illuminated 6 wt % Ag/α-Al_2O_3 catalyst was highly consistent with previous macroscopic thermocouple-based temperature measurements for the identical catalyst, reactor setup, and illumination conditions.[7] Since the thermocouple measurements average over a large volume relative to the size of plasmonic nanoparticles, it is fair to assume that for these systems the thermocouple mainly reflects the α-Al_2O_3 support temperature.

Anti-Stokes Raman Nanothermometry for Evaluating the Local Nanoparticle Temperature ($T_{nanoparticle}$) with and without Molecules Anchored on the Nanoparticle.

The analysis of the data in Figure 2 led us to postulate that the light energy is highly localized at Ag nanoparticles and that under these reaction conditions the energy flow, in the form of heat transfer from Ag to α-Al_2O_3, does not take place to a significant degree. To assess this hypothesis further, we probed the local temperature of the Ag nanoparticles ($T_{nanoparticle}$) using anti-Stokes Raman nanothermometry.[21,25] We characterized nanoparticle temperatures at a range of Raman laser intensities to understand the influence of light intensity on the Ag heating. These measurements were conducted at room temperature (~22 °C), with no external heat source applied to the catalyst. The laser intensity was varied by focusing a constant power (13 mW) laser beam to a range of spot sizes, which allows us to diffuse the beam and therefore manipulate the light intensity between 0 and ~7.5 W/cm^2. We used a 532 nm laser to probe the sample, as this laser wavelength overlaps closely with the plasmon peak of the Ag catalyst system. We also evaluated the effect of an inert N_2 gas flowing over the catalyst to understand the influence of convective heat removal on the local nanoparticle temperature.

Anti-Stokes Raman nanothermometry relies on employing anti-Stokes Raman spectrometry to measure the nanoparticle electron−phonon temperature.[21,25] It has been shown that the background in the anti-Stokes spectrum can be correlated to temperature by leveraging the electronic Fermi−Dirac distribution and its dependence on temperature. The theory that governs anti-Stokes Raman nanothermometry measurements is described in more detail in the Supporting Information and in earlier works.[8,21] In short, the inelastic anti-Stokes Raman scattering process yields anti-Stokes shifted photons that generate the background signal. This background signal can be correlated to the electronic temperature of the metal nanoparticle via the Fermi−Dirac distribution.[25] Using

https://doi.org/10.1021/jacs.4c10395
J. Am. Chem. Soc. 2024, 146, 29656−29663

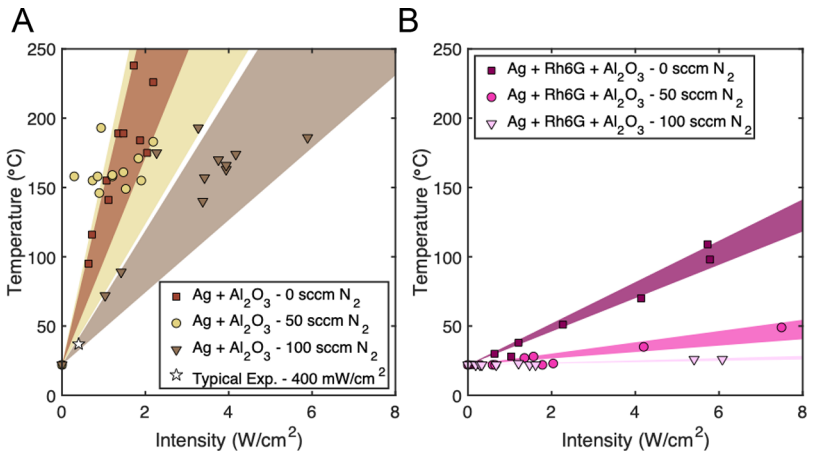

Figure 3. Raman anti-Stokes nanothermometry data. Comparing $T_{nanoparticle}$ of the Ag nanoparticle catalyst system (A) without and (B) with the presence of Rh6G on the nanoparticles shows that the local temperature of the nanoparticle can change significantly. Data were collected at room macroscopic temperature, ~22 °C. Shaded regions represent the 95% confidence intervals for the lines of best fit for each individual data set corresponding to different N_2 flow rates.

this approach, we calculated $T_{nanoparticle}$ from the exponential fit of the anti-Stokes background. Temperature measured using this approach is effectively the electron−phonon temperature of the nanoparticle. Since electronic modes equilibrate with phonon modes on a time scale of picoseconds,[21] compared to a measurement time of tens of seconds, this temperature is effectively a local, phononic temperature of the nanoparticle. An example calculation is provided in the Supporting Information.

The data in Figure 3A show the measured steady-state temperature of clean Ag nanoparticles on the Ag/α-Al_2O_3 catalyst (with no molecules adsorbed on the catalyst) under constant laser illumination, as a function of the laser intensity, and under varying flow rates of inert N_2 which convectively removes heat from the system. Each data point is a unique measurement over a single sample area, in which the Raman instrument averages two readings from the same sample spot. After one spot was measured by the laser, we moved to other spots on the catalyst sample so that we could sample different areas and avoid resampling potentially degraded areas after extended laser exposure times. We note that there is a significant amount of scatter in the data, which can be attributed to several phenomena. These include but may not be limited to sampling different clusters of Ag nanoparticles (i.e., sampling larger or denser nanoparticle clusters may result in a greater amount of local heating), heterogeneity in how the laser samples and scatters off of the rounded surface of the sifted catalyst particles, and variation in local gas flow and heat removal at the sampled site, as gas flows through local paths of least resistance. In any real-world catalyst system, for instance, nanoparticles may exist in clusters of different sizes and collective heating of these nanoparticles is a fundamental feature of the photothermal landscape. The data in Figure 3 is inclusive of this clustering (i.e., we measure the temperature of nanoparticles in the clusters). We have established through calibration measurements, where we compared the anti-Stokes Raman nanothermometry temperature measurements for a range of externally set temperatures, that the maximum error in our measurement is up to ±20 K (Figure S8).

The data in Figure 3A show that for the Ag/α-Al_2O_3 system sampled at macroscopic room temperature (~22 °C), the temperature of the nanoparticles can increase substantially, especially under high laser intensities. For example, at a laser intensity of roughly 2 W/cm^2 (~20 suns), we observe that the heating of the nanoparticle surface can be up to hundreds of degrees, depending on the extent of the flow rate of the inert N_2 gas over the sample. At the N_2 flow rates of 100 sccm, which is the flow rate typically used in our annular photoreactor studies (this is within the range of flow rates used in reactive chemical flow systems), convective heat removal from the system can substantially suppress the local nanoparticle temperature compared to lower gas flow rates.

We estimate that under the gas flow and illumination intensities employed in our typical annular photoreactor studies (i.e., 100 sccm gas flow and 400 mW/cm^2 broadband light) the local nanoparticle temperature (for particles directly under the light source), as measured using the anti-Stokes Raman nanothermometry, likely remains well below 40 °C (ΔT measured to be +15 ± 4.6 °C relative to the room temperature, the white star data point in Figure 3A). The main conclusion we can draw from the data is that the local $T_{nanoparticle}$ for a catalyst of moderate loading can be increased dramatically under very high light intensities and with no convective heat removal. On the other hand, at light intensities and convective heat removal conditions consistent with most experiments, the local nanoparticle temperature is marginally increased.

Since in catalytic reactions on nanoparticles the nanoparticles are populated with adsorbed molecules that participate in chemical reactions, we attempted to characterize how the temperature of the Ag nanoparticle may change in the presence of adsorbates. According to the above-described models of energy flow, if there are molecules on the surface of nanoparticles that when adsorbed on the nanoparticles have strong optical extinctions at the LSPR wavelengths, due to electronic excitation in the molecule or at the molecule-nanoparticles interface, the LSPR energy should preferentially flow through these excitations (as opposed to flowing through the nanoparticles) which should impact the spatial energy distribution.[17,20,21] To mimic this situation, we deposited Rh6G molecules at the surfaces of the Ag nanoparticles. While Rh6G may not perfectly emulate other reactive molecules that adsorb on plasmonic nanoparticles in traditional gas phase chemistry, we chose it because it absorbs photons with

https://doi.org/10.1021/jacs.4c10395
J. Am. Chem. Soc. 2024, 146, 29656−29663

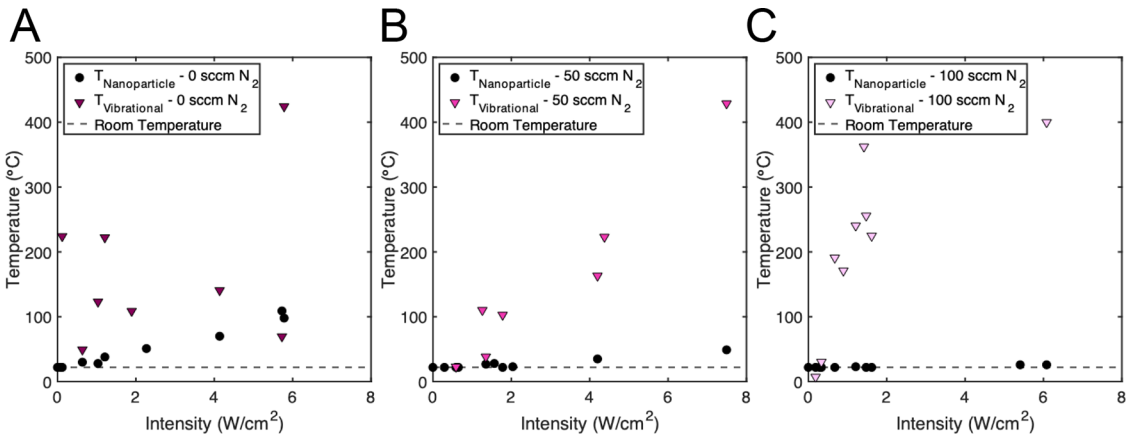

Figure 4. $T_{nanoparticle}$ and molecular $T_{vibrational}$ values as a function of laser intensity for Rh6G adsorbed on a 6 wt % Ag/α-Al_2O_3 catalyst under (A) 0 sccm N_2, (B) 50 sccm N_2, and (C) 100 sscm N_2. In all cases, the vibrational temperature of Rh6G is significantly higher than the temperature of the nanoparticle.

wavelengths close to the plasmon mode of Ag nanoparticles (of this size and clustering) which also overlaps closely with the 532 nm laser source. This matched light absorption property of Rh6G, in contrast to other reactive molecules, enabled us to obtain satisfactory Raman anti-Stokes and Stokes signals across a range of conditions. We deposited an amount of Rh6G that is sufficient to cover the Ag nanoparticles at the range of approximately one monolayer.

The optical extinction data in Figure S6B show that light interacts with Ag and Rh6G, since the extinction spectra of the Ag + Rh6G sample has features associated with both entities. Comparison of the data in Figure 3B to Figure 3A shows that, under identical conditions, the Ag nanoparticles in the Ag + Rh6G samples (Figure 3B) are at a much lower temperature than in the case of the bare nanoparticles without Rh6G (Figure 3A). This is the case for all N_2 flow rates. In the case of N_2 flow rates of 100 sccm (where we usually run our catalytic studies), the temperature of the Ag nanoparticles is almost identical to the environmental temperature, i.e., there does not seem to be local Ag nanoparticle heating.

Characterization of Molecular Adsorbate Temperatures ($T_{vibrational}$). The data in Figure 3 suggest that that the electromagnetic energy stored in the LSPR modes of the Ag nanoparticles may be preferentially dissipated through the adsorbates rather than as heat in the metal nanoparticle.[8,21] The corollary to this preferential energy flow through the molecule is that the molecular vibrational temperature should increase. To evaluate $T_{vibrational}$ of Rh6G, we utilized an experimental methodology outlined in the Supporting Information.[8,21,27−29] Briefly, properly calibrated ratios of the measured anti-Stokes to Stokes Raman peak intensities of a Rh6G vibrational mode gives us information about the $T_{vibrational}$ of the mode. This is because the peak intensity ratio depends upon the relative populations of Rh6G molecules in the vibrationally excited state (corresponding to the anti-Stokes intensity) and the ground state (corresponding to the Stokes intensity). The Boltzmann distribution function directly relates the vibrational temperature of this mode to these relative distributions and can be used to calculate the temperature of a vibrational mode within Rh6G adsorbed on our Ag nanoparticle surfaces.

Using this approach, we examined changes to the most prominent (highest intensity) characteristic Raman peak for the Rh6G molecule under 532 nm laser intensity. This was a vibrational mode at 610 cm^{-1}, which corresponds to a C−C−C in-plane vibration of Rh6G (Figure S7).[34] The data in Figure 4 show simultaneously measured values for $T_{nanoparticle}$ (obtained using Raman anti-Stokes nanothermometry as described above) and the vibrational temperatures of Rh6G ($T_{vibrational}$) at different N_2 gas flow rates between 0 and 100 sccm N_2. For all flow rates, for nanoparticles capped with Rh6G, the value of $T_{nanoparticle}$ hovers relatively close to room temperature (black circles). However, the value of $T_{vibrational}$ for the Rh6G C−C−C in-plane vibrational stretch can be tens or hundreds of degrees higher than the nanoparticle temperature, depending on the light intensity. These discrepancies between $T_{nanoparticle}$ and $T_{vibrational}$ support the hypothesis that the LSPR energy is preferentially dissipated through the adsorbed molecule and that the nanoparticle serves to localize this energy and effectively transfer it to the molecule (an antenna effect). From the data, we can estimate that under 100 sccm flow (our typical operating conditions for gas-phase chemistry in the annular reactor) at around 400 mW/cm^2, the adsorbates that are directly bonded to the nanoparticles, under resonant conditions, could be heating the equivalent of tens of degrees or more while the nanoparticle is effectively unheated. We note that the extent of heat removal from convection under reaction conditions will depend on the gas composition, where a substrate gas with better heat transfer characteristics will likely result in smaller temperature gradients. In this specific case, the heat capacity of N_2 is not very different from that of the H_2 and C_2H_4 reactive substrate. We also observe that the vibrational temperatures plotted in Figure 4C seem to be consistently higher than those in Figure 4B, despite being measured at a higher flow rate of N_2. We attribute this to a lower than ideal level of precision of the vibrational temperature measurement, as evidenced from the scattering of data presented. Nonetheless, our data in Figure 4 support the notion that the electromagnetic energy (captured in the LSPR modes) is preferentially directed through the adsorbed molecule. The fundamental physical reason for this effect is that there are available electronic excitations associated with the molecule/nanoparticles interface (i.e., the local imaginary dielectric function is high) and the energy of LSPR is localized to the nanoparticle's surface in the form of the local electric fields.[7,8,18,20−22,35] Under higher light intensities, these reactants could reach hundreds of degrees of heating as energy is shuttled into the molecule, which may be responsible for the

https://doi.org/10.1021/jacs.4c10395
J. Am. Chem. Soc. 2024, 146, 29656−29663

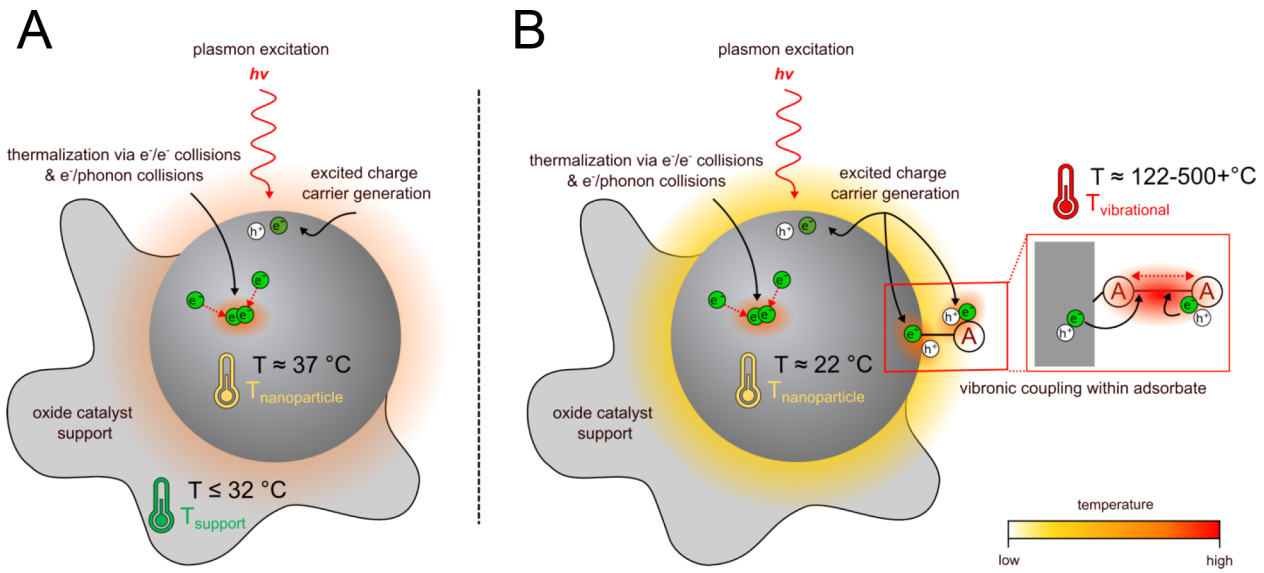

Figure 5. Temperatures of interest in plasmonic catalysts. We depict LSPR relaxation pathways and the temperature gradients that can emerge as a consequence of the relaxation in open reactive systems, with specific values for the case studies described throughout this work. (A) In the absence of an adsorbate, the nanoparticle may heat mildly (e.g., on the order of tens of degrees at 400 mW/cm^2 illumination), while the support material experiences minimal heating. (B) In the presence of adsorbates that absorb near the LSPR excitation energy, the nanoparticle can experience negligible heating while adsorbates are selectively heated—up to several hundreds of degrees for moderate to high (∼400−8000 mW/cm^2) light intensities.

large reaction rate enhancements that we often observe for these metal-molecule systems under illumination.

In summary, we studied the temperature distribution in three-dimensional supported Ag plasmonic nanoparticle catalysts under steady state catalytic conditions of constant illumination and convective heat transport. This work offers new insight into how electromagnetic energy flows throughout these materials, and how it can be directed to different components of the catalyst. We find that under illumination, the local temperature of the plasmonic nanoparticles and the catalyst support material can be different. For most conventional plasmonic catalysts systems (with a moderate illumination intensity of ∼400 mW/cm^2), characterized by low nanoparticle loading on a three-dimensional optically inert support, the plasmonic nanoparticles may heat mildly but do not induce significant heating of the support (Figure 5A). We also observe that these particles can undergo more significant localized heating under high illumination intensities when no convective heat removal is applied. Perhaps most importantly, we find that if absorbates are introduced on plasmonic nanoparticles, as long as these adsorbates offer pathways for the dissipation of electromagnetic energy (i.e., available electronic excitations at LSPR frequencies), the energy will preferentially flow through the adsorbates. Even at low to moderate light intensities, the electronic excitations in the adsorbates (or at the adsorbate-nanoparticle interface) can result in selective heating of the adsorbate by tens to hundreds of degrees (Figure 5B). These findings suggest that temperature gradients are the fundamental feature of plasmonic catalytic systems not exhibited by conventional thermal catalysts, and that it is in principle possible to have conditions where the reactants, nanoparticles, and support are at different temperatures. Furthermore, the data supports the notion that electronic excitations (driven by local LSPR-induced electric fields) facilitate these heating processes, which, in contrast to convective or infrared heating, may be fundamentally responsible for the onset of catalytic activity on illuminated plasmonic nanoparticles.

CONCLUSIONS

Plasmonic catalysts, typically comprised of networks of plasmonic nanoparticles firmly anchored on optically and chemically inert oxide supports, employ light as the driving force for chemical reactions. In this contribution, we studied the path that electromagnetic energy from visible light follows at the nanoscale within these systems, ultimately leading to chemical transformations. We address this question by devising methodologies to assess spatial temperature distributions in plasmonic catalysts. These methods encompass the localized temperatures of adsorbed molecules on catalytically active plasmonic nanoparticles, the nanoparticles themselves, and the immediate surroundings of these particles under continuous wave illumination. Our findings reveal the presence of substantial temperature gradients during steady state conditions, wherein the local temperatures of molecules, nanoparticles, and the surrounding environment exhibit pronounced variations. These temperature gradients emerge as an inherent characteristic of plasmonic catalysts, arising naturally from the mechanisms of plasmon relaxation, which involves the conversion of electromagnetic light energy, electronic excitations in plasmonic materials, and the consequent heating of various components through electronic excitation relaxation.

ASSOCIATED CONTENT

Supporting Information

The Supporting Information is available free of charge at https://pubs.acs.org/doi/10.1021/jacs.4c10395.

Raman spectroscopy (including methodology and calibration data), reactor design, catalyst synthesis, and reaction selection; additional characterization of the light

https://doi.org/10.1021/jacs.4c10395
J. Am. Chem. Soc. 2024, 146, 29656−29663

source used, Rh6G molecules in solution, and the Rh6G-modified catalyst (PDF)

AUTHOR INFORMATION

Corresponding Author

Suljo Linic − *Department of Chemical Engineering and Catalysis Science and Technology Institute, University of Michigan, Ann Arbor, Michigan 48109, United States;* orcid.org/0000-0003-2153-6755; Email: linic@umich.edu

Authors

Rachel C. Elias − *Department of Chemical Engineering and Catalysis Science and Technology Institute, University of Michigan, Ann Arbor, Michigan 48109, United States;* orcid.org/0000-0002-1085-8372

Bill Yan − *Department of Chemical Engineering and Catalysis Science and Technology Institute, University of Michigan, Ann Arbor, Michigan 48109, United States;* orcid.org/0009-0004-4602-2093

Complete contact information is available at: https://pubs.acs.org/10.1021/jacs.4c10395

Notes

The authors declare no competing financial interest.

ACKNOWLEDGMENTS

The work was supported by the National Science Foundation (NSF) (CHE-2349887). Secondary support was provided by the U.S. Department of Energy, Office of Science, Office of Basic Energy Sciences, (DE-SC0021362) (analysis of optical interactions of materials with light) and the Office of Basic Energy Science, Division of Chemical Sciences (DE-SC0021008) (materials synthesis). The authors acknowledge the financial support of the University of Michigan College of Engineering and technical support from the Michigan Center for Materials Characterization.

REFERENCES

(1) Christopher, P.; Xin, H.; Linic, S. Visible-Light-Enhanced Catalytic Oxidation Reactions on Plasmonic Silver Nanostructures. *Nature Chem.* **2011**, *3* (6), 467−472.

(2) Mukherjee, S.; Libisch, F.; Large, N.; Neumann, O.; Brown, L. V.; Cheng, J.; Lassiter, J. B.; Carter, E. A.; Nordlander, P.; Halas, N. J. Hot Electrons Do the Impossible: Plasmon-Induced Dissociation of H2 on Au. *Nano Lett.* **2013**, *13* (1), 240−247.

(3) Aslam, U.; Rao, V. G.; Chavez, S.; Linic, S. Catalytic Conversion of Solar to Chemical Energy on Plasmonic Metal Nanostructures. *Nature Catalysis* **2018**, *1* (9), 656−665.

(4) Kale, M. J.; Avanesian, T.; Christopher, P. Direct Photocatalysis by Plasmonic Nanostructures. *ACS Catal.* **2014**, *4* (1), 116−128.

(5) Cortés, E.; Xie, W.; Cambiasso, J.; Jermyn, A. S.; Sundararaman, R.; Narang, P.; Schlücker, S.; Maier, S. A. Plasmonic Hot Electron Transport Drives Nano-Localized Chemistry. *Nat. Commun.* **2017**, *8*, No. 14880.

(6) Baffou, G.; Bordacchini, I.; Baldi, A.; Quidant, R. Simple Experimental Procedures to Distinguish Photothermal from Hot-Carrier Processes in Plasmonics. *Light: Science & Applications* **2020**, *9* (1), 108.

(7) Elias, R. C.; Linic, S. Elucidating the Roles of Local and Nonlocal Rate Enhancement Mechanisms in Plasmonic Catalysis. *J. Am. Chem. Soc.* **2022**, *144* (43), 19990−19998.

(8) Boerigter, C.; Campana, R.; Morabito, M.; Linic, S. Evidence and Implications of Direct Charge Excitation as the Dominant Mechanism in Plasmon-Mediated Photocatalysis. *Nat. Commun.* **2016**, *7* (1), 1−9.

(9) Dubi, Y.; Sivan, Y. Hot" Electrons in Metallic Nanostructures—Non-Thermal Carriers or Heating? *Light: Science & Applications* **2019**, *8* (1), 1−8.

(10) Zhang, X.; Li, X.; Reish, M. E.; Zhang, D.; Su, N. Q.; Gutiérrez, Y.; Moreno, F.; Yang, W.; Everitt, H. O.; Liu, J. Plasmon-Enhanced Catalysis: Distinguishing Thermal and Nonthermal Effects. *Nano Lett.* **2018**, *18* (3), 1714−1723.

(11) Besteiro, L. V.; Kong, X.-T.; Wang, Z.; Hartland, G.; Govorov, A. O. Understanding Hot-Electron Generation and Plasmon Relaxation in Metal Nanocrystals: Quantum and Classical Mechanisms. *ACS Photonics* **2017**, *4* (11), 2759−2781.

(12) Liu, J. G.; Zhang, H.; Link, S.; Nordlander, P. Relaxation of Plasmon-Induced Hot Carriers. *ACS Photonics* **2018**, *5* (7), 2584−2595.

(13) Brown, A. M.; Sundararaman, R.; Narang, P.; Goddard, W. A.; Atwater, H. A. Nonradiative Plasmon Decay and Hot Carrier Dynamics: Effects of Phonons, Surfaces, and Geometry. *ACS Nano* **2016**, *10* (1), 957−966.

(14) Sundararaman, R.; Narang, P.; Jermyn, A. S.; Goddard, W. A., III; Atwater, H. A. Theoretical Predictions for Hot-Carrier Generation from Surface Plasmon Decay. *Nat. Commun.* **2014**, *5* (1), 5788.

(15) Yannouleas, C.; Broglia, R. A. Landau Damping and Wall Dissipation in Large Metal Clusters. *Annals of Physics* **1992**, *217* (1), 105−141.

(16) Christopher, P.; Xin, H.; Marimuthu, A.; Linic, S. Singular Characteristics and Unique Chemical Bond Activation Mechanisms of Photocatalytic Reactions on Plasmonic Nanostructures. *Nat. Mater.* **2012**, *11* (12), 1044−1050.

(17) Aslam, U.; Chavez, S.; Linic, S. Controlling Energy Flow in Multimetallic Nanostructures for Plasmonic Catalysis. *Nat. Nanotechnol.* **2017**, *12* (10), 1000−1005.

(18) Chavez, S.; Aslam, U.; Linic, S. Design Principles for Directing Energy and Energetic Charge Flow in Multicomponent Plasmonic Nanostructures. *ACS Energy Lett.* **2018**, *3* (7), 1590−1596.

(19) Chavez, S.; Rao, V. G.; Linic, S. Unearthing the Factors Governing Site Specific Rates of Electronic Excitations in Multicomponent Plasmonic Systems and Catalysts. *Faraday Discuss.* **2019**, *214*, 441−453.

(20) Linic, S.; Chavez, S.; Elias, R. Flow and Extraction of Energy and Charge Carriers in Hybrid Plasmonic Nanostructures. *Nat. Mater.* **2021**, *20*, 916−924.

(21) Boerigter, C.; Aslam, U.; Linic, S. Mechanism of Charge Transfer from Plasmonic Nanostructures to Chemically Attached Materials. *ACS Nano* **2016**, *10* (6), 6108−6115.

(22) Linic, S.; Aslam, U.; Boerigter, C.; Morabito, M. Photochemical Transformations on Plasmonic Metal Nanoparticles. *Nat. Mater.* **2015**, *14* (6), 567−576.

(23) Sinfelt, J. H. Kinetics of Ethylene Hydrogenation over Alumina. *J. Phys. Chem.* **1964**, *68* (2), 232−237.

(24) Baffou, G. Anti-Stokes Thermometry in Nanoplasmonics. *ACS Nano* **2021**, *15*, 5785.

(25) Hugall, J. T.; Baumberg, J. J. Demonstrating Photoluminescence from Au Is Electronic Inelastic Light Scattering of a Plasmonic Metal: The Origin of SERS Backgrounds. *Nano Lett.* **2015**, *15* (4), 2600−2604.

(26) Chikkaraddy, R.; de Nijs, B.; Benz, F.; Barrow, S. J.; Scherman, O. A.; Rosta, E.; Demetriadou, A.; Fox, P.; Hess, O.; Baumberg, J. J. Single-Molecule Strong Coupling at Room Temperature in Plasmonic Nanocavities. *Nature* **2016**, *535* (7610), 127−130.

(27) Brandt, N. C.; Keller, E. L.; Frontiera, R. R. Ultrafast Surface-Enhanced Raman Probing of the Role of Hot Electrons in Plasmon-Driven Chemistry. *J. Phys. Chem. Lett.* **2016**, *7* (16), 3179−3185.

(28) Warkentin, C. L.; Yu, Z.; Sarkar, A.; Frontiera, R. R. Decoding Chemical and Physical Processes Driving Plasmonic Photocatalysis Using Surface-Enhanced Raman Spectroscopies. *Acc. Chem. Res.* **2021**, *54* (10), 2457−2466.

(29) Keller, E. L.; Frontiera, R. R. Ultrafast Nanoscale Raman Thermometry Proves Heating Is Not a Primary Mechanism for Plasmon-Driven Photocatalysis. *ACS Nano* **2018**, *12* (6), 5848−5855.

(30) Christopher, P.; Linic, S. Shape- and Size-Specific Chemistry of Ag Nanostructures in Catalytic Ethylene Epoxidation. *ChemCatChem.* **2010**, *2* (1), 78−83.
(31) Aslam, U.; Linic, S. Kinetic Trapping of Immiscible Metal Atoms into Bimetallic Nanoparticles through Plasmonic Visible Light-Mediated Reduction of a Bimetallic Oxide Precursor: Case Study of Ag−Pt Nanoparticle Synthesis. *Chem. Mater.* **2016**, *28* (22), 8289−8295.
(32) Hindin, S. G.; Weller, S. W. The Effect of Pretreatment on the Activity of Gamma-Alumina I. Ethylene Hydrogenation. *J. Phys. Chem.* **1956**, *60* (11), 1501−1506.
(33) Elias, R. C.; Linic, S. Photoreactor for Photocatalysis, Related Systems, and Related Methods. US20240091732A1, 2024. https://patents.google.com/patent/US20240091732A1/en (accessed 2024−05−23).
(34) Childs, A.; Vinogradova, E.; Ruiz-Zepeda, F.; Velazquez-Salazar, J. J.; Jose-Yacaman, M. Biocompatible Gold/Silver Nanostars for Surface-Enhanced Raman Scattering. *J. Raman Spectrosc.* **2016**, *47* (6), 651−655.
(35) Zhang, J.; Guan, M.; Lischner, J.; Meng, S.; Prezhdo, O. V. Coexistence of Different Charge-Transfer Mechanisms in the Hot-Carrier Dynamics of Hybrid Plasmonic Nanomaterials. *Nano Lett.* **2019**, *19* (5), 3187−3193.

https://doi.org/10.1021/jacs.4c10395
J. Am. Chem. Soc. 2024, 146, 29656−29663